AIP | Applied Physics Letters

Waveguide-coupled detector in zero-change complementary metal–oxide–semiconductor

L. Alloatti, S. A. Srinivasan, J. S. Orcutt, and R. J. Ram

Citation: Applied Physics Letters **107**, 041104 (2015); doi: 10.1063/1.4927393
View online: http://dx.doi.org/10.1063/1.4927393
View Table of Contents: http://scitation.aip.org/content/aip/journal/apl/107/4?ver=pdfcov
Published by the AIP Publishing

Waveguide-coupled detector in zero-change complementary metal–oxide–semiconductor

L. Alloatti,[a] S. A. Srinivasan,[b] J. S. Orcutt,[c] and R. J. Ram
Massachusetts Institute of Technology, Cambridge, Massachusetts 02139, USA

(Received 8 June 2015; accepted 14 July 2015; published online 27 July 2015)

We report a waveguide-coupled photodetector realized in a standard CMOS foundry without requiring changes to the process flow (zero-change CMOS). The photodetector exploits carrier generation in the silicon-germanium normally utilized as stressor in pFETs. The measured responsivity and 3 dB bandwidth are of 0.023 A/W at a wavelength of 1180 nm and 32 GHz at −1 V bias (18 GHz at 0 V bias). The dark current is less than 10 pA and the dynamic range is larger than 60 dB. © *2015 AIP Publishing LLC*. [http://dx.doi.org/10.1063/1.4927393]

Monolithic integration of million-transistors circuits with photonic components is an enabling technology for the high-performance computers (HPC) foreseen in the next decade.[1] However, several materials, processes, or geometries generally utilized for building photonic components are not available in advanced electronic foundries. For example, even if optical detection can be achieved by mid-band gap absorption in doped or poly-crystalline silicon waveguides or by internal photoemission absorption in Schottky junctions,[2,3] the most typical approach consists of incorporating pure germanium on silicon.[4–6] As a consequence, a complete toolbox has so far been demonstrated only in modified CMOS flows[4,5] and rely on the 90 nm or older nodes, which are no longer utilized for building HPC microprocessors.[7] The modification of existing nodes, moreover, requires costly process development and challenges fabrication yield.[8]

An alternative approach consists of designing photonic components within existing CMOS foundries without violating the original design rules and without requiring any change of the fabrication process—a term that we named "zero-change CMOS photonics."[9] In this approach, the fabrication yield of the transistors remains unaltered and enables the realization of electronic circuits of the complexity of microprocessors. Discrete optical components, such as vertically coupled photodetectors, have been fabricated in zero-change CMOS in various foundries.[10,11] Within the 45 nm, 12SOI silicon-on-insulator CMOS node of IBM, we have recently demonstrated zero-change fabrication of grating couplers (GCs), waveguide propagation losses of less than 5 dB/cm in the 1170 nm–1250 nm range, and 5 Gbps 70 fJ optical transmitter comprising modulator and driver.[9,12] This node, moreover, is at the core of the 3rd, 4th, and 5th most performing computers in the top 500 supercomputer list.[7]

In this work, we demonstrate a waveguide-coupled photodetector realized in 45 nm 12SOI, therefore, completing a photonic toolbox within a zero-change CMOS paradigm. Previous work on the integration of photodetectors within zero-change CMOS has focused exclusively on surface-illuminated devices.[10,13] Nearly, all of the previous work has relied on absorption of light by crystalline silicon and has been restricted to $\lambda < 850$ nm. An exception is the demonstration of a surface-illuminated detector also at $\lambda = 850$ nm that used the silicon-germanium (SiGe) layer within an IBM bipolar transistor (BiCMOS) process.[11] Our waveguide photodetector provides a crucial interface between photonic integrated circuits and CMOS electronic integrated circuits. The waveguide detector presented here is responsive at longer wavelengths that can be guided with low loss through silicon photonic integrated circuits.

The photodetector is based on carrier generation in the SiGe heteroepitaxially grown in silicon pockets. This material is utilized in the 12SOI process for compressively straining pFET channels, therefore, increasing the hole mobility.[14,15] The optical mode and the cross section of the photodetector are shown in Fig. 1(a). On top of the crystalline silicon, a 172 nm wide polysilicon strip (normally utilized as transistor gates) defines the waveguide core. A 300 nm wide SiGe pocket is formed next to the polysilicon. Two well implants define a pn-diode whose junction is in the center of the SiGe region. The germanium content is estimated to be in the 25–35 at. % based on data of older nodes.[14] The SiGe has likely been p-type doped during epitaxy and is designed sufficiently narrow for avoiding the formation of crystal dislocations.[16] Source/drain implants, silicidation, and metal bias form the electron/hole collectors and complete the electrical circuit. Ground-signal (GS) high-frequency electrodes with minimal density of metal fill shapes (required by the foundry to minimize dishing of the wafer) are placed parallel to the waveguide (Fig. 1(b)). The waveguides have been designed by a fully scripted code which became part of a complete photonic-design automation (PDA) tool based on Cadence with abstract photonic layers, automatic DRC-cleaning, and photonic/electronic auto-routing.[17]

Photodiodes of three different SiGe lengths (1.4 μm, 9.4 μm, and 99.4 μm) have been fabricated for characterizing the optical loss (cut-back method). Each device has both an input and an output grating coupler. The current-voltage characteristic of the 99.4 μm long device with and without

[a]Electronic mail: alloatti@mit.edu
[b]Present address: Photonics Research Group, Department of Information Technology, Ghent University – Imec, St. Pietersnieuwstraat 41, 9000 Ghent, Belgium.
[c]Present address: IBM T.J. Watson Research Center, 1101 Kitchawan Rd., Yorktown Heights, New York 10598, USA.

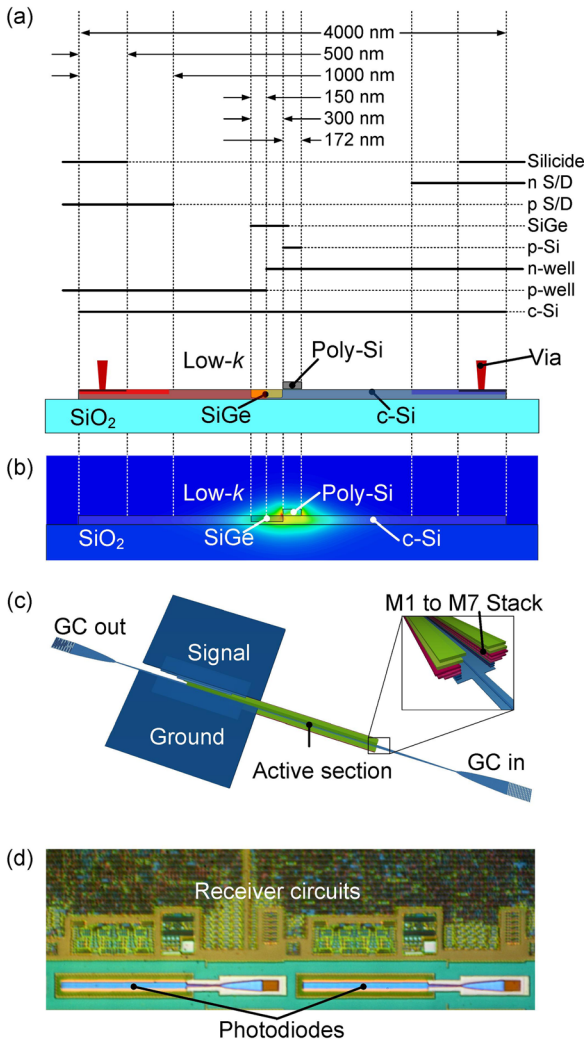

FIG. 1. Cross-section, optical mode, and geometry of the photodetector. (a) Schematic cross-section of the photodiode and of the mask-set used to generate it. The optical mode is guided by the rib-waveguide structure consisting of a 4 μm wide, 80 nm thick crystalline silicon and a 172 nm wide, 65 nm thick polysilicon core. On one side of the polysilicon, 300 nm wide SiGe is grown by heteroepitaxy. Light is coupled in and out of the waveguide through GCs. (b) Representation of the intensity of the TE_{00} optical mode. (c) View of the photodetector with 99.4 μm-long SiGe active region. GS electrodes are located parallel to the waveguide. The first seven metal layers are present along the entire device length (inset). (d) Photograph the fabricated device monolithically integrated with an electric receiver.[22]

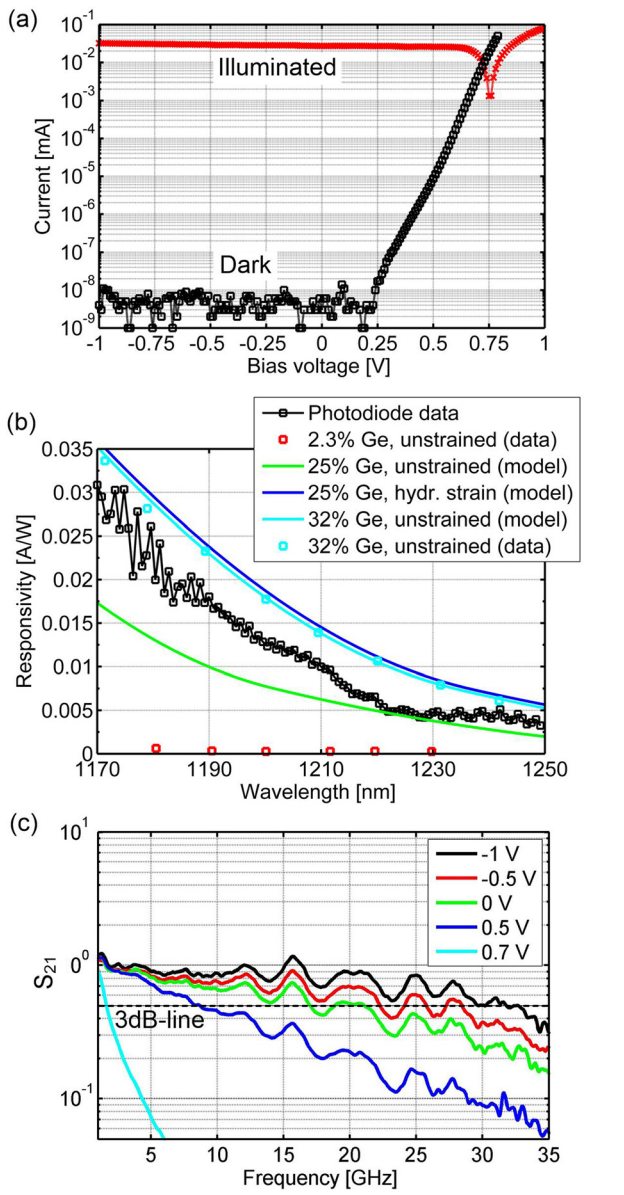

FIG. 2. Device performance. (a) Current-voltage characteristics with and without illumination. Under illumination, the zero-current voltage is 0.75 V, and the photocurrent is 32 μA at -1 V bias with 1.4 mW in-waveguide optical power (wavelength of 1180 nm). The dynamic range is larger than 60 dB. (b) Responsivity vs. wavelength and the responsivity for strained and unstrained SiGe at different concentrations based on experimental data[18] and on the Macfarlane equations (legend). The model curves (legend) use the following parameters: energy gap $E_g = 0.991$ eV and 0.965 eV and phonon energy $\vartheta = 480$ K and 460.4 K for unstrained alloys with 25% and 32% germanium content, respectively (legend). The model for strained silicon-germanium is obtained by shrinking the bandgap by 0.03 eV. (c) Frequency response. A 3 dB bandwidth of 18 GHz is obtained at 0 V bias and of 32 GHz at -1 V bias.

illumination is given in Fig. 2(a). The dark current is less than 10 pA resulting to a reverse-bias dynamic range of more than 60 dB. The responsivity of the device (defined as optical power at the photodiode input/photocurrent) was measured as a function of wavelength by recording at the same time input and output optical power and photocurrent (Fig. 2(b)). The measurement was repeated a second time with exchanged input and output fiber connectors such as to verify that the input and output grating couplers caused the same optical loss. For comparison, Fig. 2(b) reports also the responsivity based on the optical absorption measured in unstressed SiGe at various germanium concentrations[18] and based on the Macfarlane equations

$$\alpha(\nu) = A\left[\frac{(h\nu - E_g - k\theta)^2}{1 - e^{-\theta/T}} + \frac{(h\nu - E_g + k\theta)^2}{e^{\theta/T} - 1}\right],$$

where ν is the photon frequency, E_g is the energy gap, k is the Boltzmann constant, $T = 295$ K is the room temperature, ϑ is the phonon energy (expressed in K), and the sum over the six branches of the vibrational spectrum has already been carried out and is contained in the coefficient A. For the bandgap and phonon energy of unstrained SiGe, we set $E_g = 1.088$ eV, 0.991 eV, and 0.965 eV and $\vartheta = 550$ K, 480 K, and 460.4 K for the concentrations of 0%, 25%, and 32%, respectively. The bandgap data and the phonon energy for pure silicon are as reported by Braunstein.[18] With these

values, good agreement is obtained with the experimental data[18] of unstrained silicon germanium. The effects of hydrostatic strain[19] on 25% germanium are taken into account by shrinking the bandgap by 0.03 eV (Fig. 2(b)), obtaining an upper boundary of the measured responsivity.

To determine the device responsivity based on the absorption coefficient of silicon-germanium, we calculated the power overlap integral of the optical mode with the SiGe region. The overlap integral is found to vary approximately linearly between 0.128 at a wavelength of 1170 nm and 0.121 at a wavelength of 1250 nm. At the wavelength of 1180 nm, the responsivity is 0.023 ± 0.002 A/W (−1 V bias). If no other loss mechanism was present, this responsivity would correspond to an optical propagation loss of 10.7 dB/cm. From the cut-back method, the optical loss was found to be 40 ± 10 dB/cm and is dominated by free-carrier absorption (FCA) in the pre-doped poly-silicon. This means that the quantum efficiency of the present geometry can reach at least 20% in the long-device limit. Furthermore, results in a 0.18 μm bulk CMOS node[20] show that the propagation loss of optimized polysilicon waveguides can be as low as 10 dB/cm. Because of the small optical overlap with the polysilicon rib of the current geometry (Fig. 1), the use of low-loss poly-silicon (in a modified process) could lead to parasitic losses below 10 dB/cm (Ref. 21) and therefore to quantum efficiencies beyond 50% in the long device limit.

An alternative scheme for increasing the responsivity of the photodiode consists of using resonant structures such as rings. This approach would have multiple advantages: first, the current scheme of detecting wavelength-division multiplexing (WDM) signals (based on a silicon ring acting like a filter and a separate photodiode) would be simplified by the elimination of the drop port.[22] Second, the effective optical path length would be dramatically increased without sacrificing space. Third, the use of whispering gallery modes would no longer require the use of poly-silicon, therefore eliminating the parasitic loss dominated by the latter. Finally, by using, for example, a ring with a radius of 5 μm,[12] the total junction length would be decreased leading to a smaller capacitance. The problem of locking the resonator to the correct wavelength with an on-chip feedback loop has, moreover, been recently addressed.[22]

The bandwidth of the device was measured by contacting the GS electrodes with a 50 μm pitch GS probe of Cascade Microtech (model Infinity I67-A-GS-50). The reference plane was set at the V-connector of the probe, so that the probe is considered part of the photodiode. The frequency response was measured with a 40 GHz VNA (HP8722D) and the frequency-response of the setup (comprising modulator, semiconductor-amplifier (SOA), RF cables, and bias-T) was calibrated with a reference photodiode (Discovery Semiconductors, model DSC30-3-2010) of known frequency-response at a wavelength of 1550 nm. It was confirmed that the frequency response of the combined system of modulator and reference photodiode is identical (within measurement accuracy) at 1550 nm and 1180 nm. The photodiode has a 3 dB bandwidth of 18 GHz at 0 V bias. The bandwidth increases to 32 GHz with a reverse bias of −1 V. A different set of devices, in which the diode junction was shifted by 150 nm towards the waveguide center, showed smaller bandwidths (8 GHz at −1 V bias). The generated photocurrent is sufficient for driving the on-chip electrical receiver[23] which has a peak-to-peak sensitivity of 6 μA at 5 Gb/s.[22]

In conclusion, we have fabricated and characterized a waveguide-coupled photodetector compatible with unchanged CMOS processes. The photodiode has a 3 dB bandwidth of 32 GHz at −1 V bias. The photodiode is realized in the 45 nm CMOS node, which is widely used in high-performance computing.

We acknowledge support by DARPA POEM under Award No. HR0011-11-C-0100 and Contract No. HR0011-11-9-0009, led by Dr. Jagdeep Shah. The views expressed are those of the authors and do not reflect the official policy or position of the DoD or the U.S. Government.

[1]P. W. Coteus, J. U. Knickerbocker, C. H. Lam, and Y. A. Vlasov, IBM J. Res. Dev. **55**(5), 14:1 (2011).
[2]M. W. Geis, S. J. Spector, M. E. Grein, R. T. Schulein, J. U. Yoon, D. M. Lennon, S. Deneault, F. Gan, F. X. Kaertner, and T. M. Lyszczarz, IEEE Photonics Technol. Lett. **19**(3), 152 (2007).
[3]M. Casalino, Int. J. Opt. Appl. **2**(1), 1 (2012).
[4]S. Assefa, S. Shank, W. Green, M. Khater, E. Kiewra, C. Reinholm, S. Kamlapurkar, A. Rylyakov, C. Schow, F. Horst, H. P. Pan, T. Topuria, P. Rice, D. M. Gill, J. Rosenberg, T. Barwicz, M. Yang, J. Proesel, J. Hofrichter, B. Offrein, X. X. Gu, W. Haensch, J. Ellis-Monaghan, and Y. Vlasov, IEEE Int. Electron Devices Meet. **2012**, 33.8.
[5]F. Boeuf, S. Cremer, E. Temporiti, M. Fere, M. Shaw, N. Vulliet, O. bastien, D. Ristoiu, A. Farcy, T. Pinguet, A. Mekis, G. Masini, P. Sun, Y. Chi, H. Petiton, S. Jan, J.-R. Manouvrier, C. Baudot, P. Le-Maitre, J. F. Carpentier, L. Salager, M. Traldi, L. Maggi, D. Rigamonti, C. Zaccherini, C. Elemi, B. Sautreuil, and L. Verga, in *Optical Fiber Communication Conference* (OSA, 2015), Paper No. W3A.1.
[6]L. Vivien, A. Polzer, D. Marris-Morini, J. Osmond, J. M. Hartmann, P. Crozat, E. Cassan, C. Kopp, H. Zimmermann, and J. M. Fedeli, Opt. Express **20**(2), 1096 (2012).
[7]See http://www.top500.org for Pos. 1: Tianhe-2, Guangzhou, China; Pos.2: Titan, Ridge National Lab., USA; Pos. 3: Sequoia, DOE, USA; Pos. 4: K computer, RIKEN, Japan; and Pos. 5: Mira, DOE, USA, November 2014, Top500.
[8]H. Byun, J. Bok, K. Cho, K. Cho, H. Choi, J. Choi, S. Choi, S. Han, S. Hong, S. Hyun, T. J. Jeong, H.-C. Ji, I.-S. Joe, B. Kim, D. Kim, J. Kim, J.-K. Kim, K. Kim, S.-G. Kim, D. Kong, B. Kuh, H. Kwon, B. Lee, H. Lee, K. Lee, S. Lee, K. Na, J. Nam, A. Nejadmalayeri, Y. Park, S. Parmar, J. Pyo, D. Shin, J. Shin, Y.-h. Shin, S.-D. Suh, H. Yoon, Y. Park, J. Choi, K.-H. Ha, and G. Jeong, Photonics Res. **2**(3), A25 (2014).
[9]J. S. Orcutt, A. Khilo, C. W. Holzwarth, M. A. Popovic, H. Li, J. Sun, T. Bonifield, R. Hollingsworth, F. X. Kaertner, H. I. Smith, V. Stojanovic, and R. J. Ram, Opt. Express **19**(3), 2335 (2011).
[10]X. Yang and A. Babakhani, in *Optical Fiber Communication Confernce* (OSA, 2013), Paper No. OTu2C.
[11]T. Yin, A. M. Pappu, and A. B. Apsel, IEEE Photonics Technol. Lett. **18**(1), 55 (2006).
[12]J. M. Shainline, J. S. Orcutt, M. T. Wade, K. Nammari, B. Moss, M. Georgas, C. Sun, R. J. Ram, V. Stojanovic, and M. A. Popovic, Opt. Lett. **38**(15), 2657 (2013).
[13]A. Gupta, S. P. Levitan, L. Selavo, and D. M. Chiarulli, Dig. Tech. Pap. Symp. VLSI Technol. **2004**, 957–960.
[14]S. E. Thompson, M. Armstrong, C. Auth, M. Alavi, M. Buehler, R. Chau, S. Cea, T. Ghani, G. Glass, T. Hoffman, C. H. Jan, C. Kenyon, J. Klaus, K. Kuhn, Z. Y. Ma, B. McIntyre, K. Mistry, A. Murthy, B. Obradovic, R. Nagisetty, P. Nguyen, S. Sivakumar, R. Shaheed, L. Shiften, B. Tufts, S. Tyagi, M. Bohr, and Y. El-Mansy, IEEE Trans. Electron Devices **51**(11), 1790 (2004).
[15]S. Narasimha, K. Onishi, H. M. Nayfeh, A. Waite, M. Weybright, J. Johnson, C. Fonseca, D. Corliss, C. Robinson, M. Crouse *et al.*, IEEE Int. Electron Devices Meet. **2006**, 1–4.
[16]D. J. Paul, Semicond. Sci. Technol. **19**(10), R75 (2004).

[17]L. Alloatti, M. Wade, V. Stojanovic, M. Popovic, and R. J. Ram, IET Optoelcetronics **9**(4), 163–167 (2015).
[18]R. Braunstein, A. R. Moore, and F. Herman, Phys. Rev. **109**(3), 695 (1958).
[19]E. Ghahramani and J. E. Sipe, Phys. Rev. B **40**(18), 12516 (1989).
[20]R. Meade, J. S. Orcutt, K. Mehta, O. Tehar-Zahav, D. Miller, M. Georgas, B. Moss, C. Sun, Y.-H. Chen, J. Shainline, M. Wade, R. Bafrali, Z. Sternberg, G. Machavariani, G. Sandhu, M. Popovic, R. Ram, and V. Stojanovic, Dig. Tech. Pap. Symp. VLSI Technol. **2014**, 1–2.
[21]J. S. Orcutt, B. Moss, C. Sun, J. Leu, M. Georgas, J. Shainline, E. Zgraggen, H. Li, J. Sun, M. Weaver, S. Urosevic, M. Popovic, R. J. Ram, and V. Stojanovic, Opt. Express **20**(11), 12222 (2012).
[22]C. Sun, M. Wade, M. Georgas, S. Lin, L. Alloatti, B. Moss, R. Kumar, A. Atabaki, F. Pavanello, R. J. Ram, M. A. Popovic, and V. Stojanovic, Dig. Tech. Pap. Symp. VLSI Circuits **2015**, 1–2.
[23]M. Georgas, B. R. Moss, C. Sun, J. Shainline, J. S. Orcutt, M. Wade, Y. H. Chen, K. Nammari, J. C. Leu, A. Srinivasan, R. J. Ram, M. A. Popovic, and V. Stojanovic, Dig. Tech. Pap. Symp. VLSI Circuits **2014**, 1–2.